IEEE Access
Multidisciplinary | Rapid Review | Open Access Journal

Received November 5, 2019, accepted December 4, 2019, date of publication December 6, 2019,
date of current version December 23, 2019.

Digital Object Identifier 10.1109/ACCESS.2019.2958204

Optimal Carrier-Phase Integer Combinations for Modernized Triple-Frequency BDS in Precise Point Positioning

HONGLEI QIN[1], PENG LIU[1], JIAQING QU[2], AND LI CONG[1]
[1]School of Electronic and Information Engineering, Beihang University, Beijing 100191, China
[2]Shanghai Radio Equipment Research Institute, Shanghai 200233, China

Corresponding author: Li Cong (congli_bh@buaa.edu.cn)

ABSTRACT The latest generation of Global Navigation Satellite System (GNSS) satellites are transmitting signals on three or more frequencies, it brings new opportunities and challenges for data integration in Multi–GNSS Experiment (MGEX). To reduce the convergence time, less computationally intensive method is three-carrier ambiguity resolution (TCAR). But the three combinaitons can not be found in precise point positioning (PPP) yet, especially for the third generation BeiDou Navigation Satellite System (BDS-3). This contribution concentrates on the multi-frequency carrier-phase integer combinations for BDS-3 in PPP. More specifically, the triple-frequency plane is degraded to two-dimensional plane for BDS-3 under the assumption of a low observation noise. And then third frequency coefficient should be limited as a constraint, considering that inter frequency bias (IFB) is dynamic quantity. Thereafter, a new searching algorithm based on the Satisfiability Modulo Theories (SMT) is presented to search the optimal integer combinations fast. Meanwhile, ionosphere-free combinations are exhibited and are not suitable for TCAR. Futhermore, the availability of the SMT-based searching algorithm (SMTSA) is verified. Finally, the most interesting carrier-phase combinations that can be used for PPP ambiguity resolution are screened out for later research. Meanwhile, in order to give a referenced comprehensive assessment of the integer combination, some valuable combinations for BDS-3 are displayed. It provides scientific support for the triple-frequency AR which has less convergence time than dual-frequency AR. Moreover, it also gives the important and valuable reference for future research on multi-frequency ambiguity–enabled PPP.

INDEX TERMS Carrier-phase integer combinations, multi-frequency, precise point positioning, The third generation BeiDou navigation satellite system, three-carrier ambiguity resolution.

I. INTRODUCTION

Precise point positioning (PPP) utilizes dual-frequency pseudorange and carrier-phase observations in single receiver to generate high-accuracy positioning solutions by using precise satellite orbits, clock corrections and other error models [1], [2]. One major drawback of PPP is the long convergence time. It can range from tens of minutes to several hours [3].

The main problems on restricting the convergence of PPP include the ambiguities of non-integer properties. In standard PPP, the carrier-phase ambiguity is a combination of the integer ambiguity term and hardware-dependent biases originating from the satellites and receivers, thus resulting in the carrier-phase ambiguity term being a real-valued quantity. This is true for any single receiver positioning using carrier-phase measurements, which explains why PPP requires an extended convergence period to reliably estimate these ''float ambiguities''. The measures to solve the problem of the long convergence time is mainly contained the ambiguity resolution. Since 2007, a number of researchers have been making progress on the challenge of resolving carrier-phase ambiguities in PPP processing [4]–[6]. Correcting integer ambiguity-fixing can shorten the convergence time, thus it potentially improves the accuracy and consistency of PPP solutions, and enables instantaneous positioning in real time.

The most efficient method for ambiguity resolution (AR) is the least squares ambiguity decorrelation adjustment also

The associate editor coordinating the review of this manuscript and approving it for publication was Zheng H. Zhu.

known as the LAMBDA method [7]. It is characterized by a linear transformation based on the variance-covariance matrix which best decorrelates the unknown ambiguity parameters. This leads to a transformation matrix Z which always contains the optimal set of integer combinations for a given station-satellite geometry. Although bootstrapping can also be applied and performs well [8], [9]. The LAMBDA method guarantees the best success-rate performance as shown by Teunissen [10]. However, the determination of the decorrelating transformation matrix Z and subsequent integer search imposes a certain computational burden.

Less computationally intensive methods exist and work by using predefined one-to-one carrier-phase combinations that retain the integer nature of the ambiguities. In the dual frequency case, a widely used combination in AR is the wide-lane with a wavelength of 86.2 cm in Global Positioning System (GPS). Extensions to the triple frequency case include three-carrier ambiguity resolution (TCAR) developed by Forssell et al. or cascade integer resolution (CIR) proposed by Jung et al. [11], [12]. Compared with the LAMBDA method, these approaches use a predefined 3×3 transformation matrix Z, which does not take into account the correlation between the ambiguities of different satellite-pairs due to receiver-satellite geometry [13]. For this reason, the combinations are considered to be ''geometry-free'' for AR. The ambiguity-fixing is normally done using integer bootstrapping, also known as sequential rounding or cascaded AR [14].

Previous research into three-carrier combinations has been somewhat piecemeal. Odijk and Teunissen showed that adding a third frequency will drastically increase the number of possible combinations and provide further Ionosphere-Free (IF) integer combinations [15]. Han and Rizos proposed several combinations which have longer effective wavelengths and less noise [16]. Richert and El-Sheimy concentrated on the mitigation of multi-path and troposphere biases [17]. Feng summarized the mathematical model of combination in detail [18]. Gu and Li respectively analyzed performance of PPP-AR for the BeiDou Navigation Satellite System (BDS) with triple frequency data by different uncalibrated phase delay (UPD) models [19], [20]. Thereafter, Deng compared performance of pseudorange and carrier-phase combinations for BDS in PPP-AR [21]. But they are not integer carrier-phase combinations. Cocard made a systematic analysis of integer combination form and selection method for GPS in double-difference (DD) applications [22]. The optimal integer combination, which is an optimal integer combination coefficient set of an observation model with respect to the unit cycle, makes AR success rate large. Zhang made their research extend to BDS on the base of the Cocard [23]. Li further researched on the combinatorial selection method for four Global Navigation Satellite Systems (GNSS) [24]. In conclusion, the existing selection methods analyzed combination coefficient on GPS or BDS well. But there is almost no research literature on selection of combination coefficient for the third generation BDS (BDS-3). Hence, when TCAR method is used to realize PPP-AR for BDS-3, it is necessary to analyze carrier-phase integer combination.

It has been shown that explicitly accounting for the ionosphere can permit rapid or even instantaneous resolution of ambiguities after cycle slips [25]. In contrast, Geng used a method of ionospheric prediction using ambiguity-fixed parameters from the PPP solution to correct the wide-lane carrier-phase observation [26]. Collins and Bisnath showed straightforward examples of covariance analysis to explain why the ionosphere helps ambiguity resolution [27]. The ionosphere-free combinations are special for PPP. Whether they are suitable to become extra-wide-lane, wide-lane, and narrow-lane for BDS-3 in PPP is not solved.

If PPP users use the positioning model where the inter frequency bias (IFB) is derived to the third frequency P3 or L3, it is necessary to carefully consider the absolute value of coefficient of the third observation [28]. The IFB can be estimated with other unknown parameters as a time invariant constant [29]. But the time-varying part of IFB has an influence on the convergence time and positioning performance in PPP [30], [31]. IFB should be considered when combination coefficients are chosen.

Furthermore, the frequencies of BDS-3 (1575.42 MHz, 1176.45 MHz, 1268.52 MHz) are similar to those of GPS (1575.42 MHz, 1227.60 MHz, 1176.45 MHz). To search the feasible solution set, the range of coefficients are same as those in GPS. Traversal searching algorithm (TSA) will take too much time to process iterations, especially the number of feasible solutions is small when searching constraints are strict [22], [23]. How to optimize algorithm to reduce the processing time is also a valuable problem.

Aiming at four problems about ambiguity-fixing in PPP-AR, we fast select all feasible carrier-phase integer combinations which contain extra-wide-lane, wide-lane and narrow-lane. The primary contributions of this paper are summarized as follows.

1) We prove that combination coefficients can be mapped to ionosphere delay and lane-number under the assumption of a low observation noise in BDS-3. The dimensionality can be reduced by one-dimension to simplify selecting carrier-phase integer combination.
2) The IFB constraint is added to select optimized carrier-phase integer combinations, considering the influence of the variable IFB on positioning. All feasible combinations, which contain extra-wide-lane, wide-lane and narrow-lane, are selected.
3) The SMT-based searching algorithm (SMTSA) is proposed to decrease the processing time of searching task. Compared with TSA, SMTSA decreases the processing time of searching feasible solutions to 25%.
4) We find all feasible combinations for BDS-3 in PPP-AR. The ionosphere delay in PPP is so conspicuous that ionosphere-free combinations are preferred. But there are high noise and narrow-lane for the carrier-phase integer combinations with ionosphere-free.

The remainder of this paper is organized as follows. Section 2 analyzed lane-number for BDS-3 and defined the bound of lanes. Thereafter, section 3 presents the mathematical model of the lane, ionosphere, noise and IFB and simplified the dimensionality of selecting carrier-phase integer combination. Section 4 presents all searching constraints in PPP and improves the searching algorithm to decrease the processing time. Furthermore, section 5 verifies the availability of the algorithm and gives all possible combinations. Meanwhile, all feasible combinations, which contain extra-wide-lane, wide-lane and narrow-lane, are displayed. Finally, some conclusions are given in section 6.

II. PRELIMINARIES

For a single epoch observation between one satellite and one receiver, the combining undifferenced pseudorange P_c and carrier-phase L_c observation with respect to the unit meter can be expressed as follows [18].

$$P_c = \frac{(if_1)P_1 + (jf_2)P_2 + (kf_3)P_3}{if_1 + jf_2 + kf_3} \tag{1}$$

$$L_c = \frac{(if_1)L_1 + (jf_2)L_2 + (kf_3)L_3}{if_1 + jf_2 + kf_3} \tag{2}$$

The combining frequency is displayed as follows [32].

$$f_c = if_1 + jf_2 + kf_3 \tag{3}$$

According to equation (2) and (3), it has

$$\Phi_c = i\Phi_1 + j\Phi_2 + k\Phi_3 \tag{4}$$

where Φ is the carrier-phase observation with respect to the unit cycle. To use TCAR or CIR, the coefficients i, j, and k are integers to guarantee combining ambiguity as an integer.

There are four civil signals (B1I, B1C, B2a, and B3I) for BDS-3. Considering the compatibility of BDS and other GNSS systems, the B1C is used to have the same frequency as other GNSS systems. The three frequencies are 1575.42 MHz (B1C), 1176.45 MHz (B2a), and 1268.52 MHz (B3I).

$$f_i = m_i f_0 \tag{5}$$

where f_0 is the basic frequency (10.23 MHz) as same as GPS. So $m_1 = 154$, $m_2 = 115$, $m_3 = 124$, correspondingly.

According to equation (3) and (5), it can get

$$f_c = mf_0 \tag{6}$$

$$m = im_1 + jm_2 + km_3 \tag{7}$$

where m is called the lane-number [22].

The largest wide-lane has a lane-number m = 1 and a wavelength of about 29.305 m. Fig. 1 shows the wavelengths for the first 15 wide-lanes. Based on the lane-number m, combinations may be divided into four groups, compared with three groups presented by Cocard [22].

1) A extra-lane region: $0 < m < 39$. The combining wavelength is larger than the combining wavelength L_c, whose frequency is $(f_1 - f_2)$ in BDS-3.

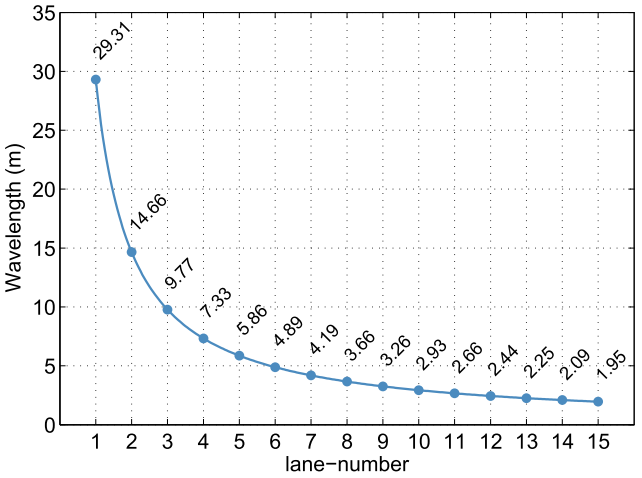

FIGURE 1. Wavelengths in meters as a function of the lane-number m for the first 15 largest wide-lanes $1 \leq m \leq 15$.

2) An wide-lane region: $39 \leq m \leq 115$. The combining wavelength is between the largest basic wavelength L2 and the combining wavelength L_c.
3) An intermediate-lane region: $115 \leq m \leq 154$. The combining wavelength is between the largest basic wavelength L2 and the smallest basic wavelength L1.
4) A narrow-lane region: $m > 154$. The combining wavelength is smaller than the smallest basic wavelength L1.

III. THE COMBINING MATHEMATICAL MODEL OF BDS-3

A. DIMENSIONALITY REDUCTION OF COMBINATION COEFFICIENTS

1) THE LANE PLANES

For a given lane-number m, there are an infinite number of combinations with the same wavelength. The triplet (i, j, k) has only to satisfy equation (7).

$$154i + 115j + 124k = m \tag{8}$$

which corresponds to the equation of a plane in the i-j-k space. The normal vector $\overline{n}_{lane}$ to the plane is given,

$$\overline{n}_{lane} = (m_1, m_2, m_3)^T = (154, 115, 124)^T \tag{9}$$

Meanwhile, the equation (8) corresponds to a linear Diophantine equation in three terms. A Diophantine equation is an equation in which only integer solutions are allowed. The equation (8) has a general solution given by,

$$\begin{bmatrix} i \\ j \\ k \end{bmatrix} = \begin{bmatrix} 1 & 23 & 9 \\ 17 & -6 & 154 \\ -17 & -23 & -154 \end{bmatrix} \begin{bmatrix} m \\ \alpha \\ \beta \end{bmatrix} \tag{10}$$

where α and β are arbitrary integers.

Geometrically, all m-plane are parallel. The shortest distance between two consecutive planes is $\delta = \|\overline{n}_{lane}\|^{-1} \approx 0.00437$. Symmetrical to the central zero lane plane (m=0), they are located at constant distances of the planes having a lane-number of -m and m, respectively. Fig. 2 illustrates this situation. In addition, in every plane the integer combinations

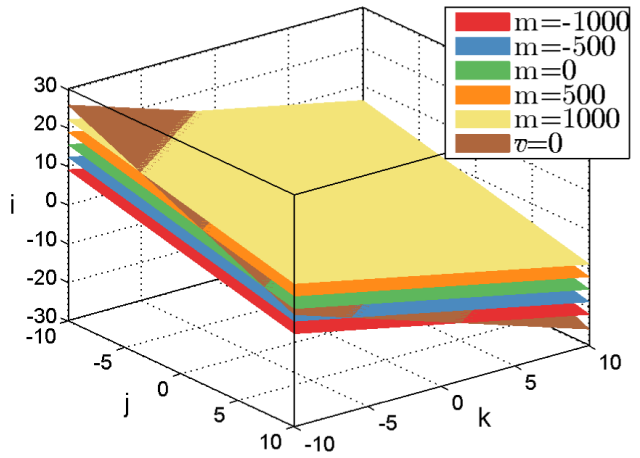

FIGURE 2. m-Planes for m=0, ±500, ±1000 and the ionosphere-free plane in the i-j-k space for a cuboid with dimension [±10, ±10, ±30].

are on a regularly spaced grid, where the spacing is always the same and given by the two vectors $(23, -6, 23)^T$ and $(9, 154, -154)^T$.

2) THE IONOSPHERE PLANES

The first order of the combination ionosphere noise is shown.

$$I_c = -f_1^2 \frac{i/f_1 + j/f_2 + k/f_3}{if_1 + jf_2 + kf_3} I_1 \tag{11}$$

$$\nu = -f_1^2 \frac{i/f_1 + j/f_2 + k/f_3}{if_1 + jf_2 + kf_3} \tag{12}$$

$$\overline{\nu} = f_1(i/f_1 + j/f_2 + k/f_3) \tag{13}$$

where ν is the ionosphere amplification factor with respect to meter (IAFM), $\overline{\nu}$ is the ionosphere amplification factor with respect to cycle (IAFC).

In PPP, we should guarantee the ionosphere is eliminated in every step for the one-to-one ambiguity resolution (e. g., TCAR and CIR). This is the most important issue for PPP instantaneous or rapid ambiguity-fixing [33], [34]. That is to say, we can get an ionosphere-free plane according to equation (11), any integer pairs (i, j, k) should in this plane.

The IAFC $\overline{\nu}$ can be converted to an equation about lane-number.

$$\overline{\nu} = m_1(i/m_1 + j/m_2 + k/m_3) \tag{14}$$

Namely,

$$7130i + 9548j + 8855k = 7130\overline{\nu} = \overline{\nu_i} \tag{15}$$

Equation (15) corresponds again to a set of parallel planes in the i-j-k space. The central plane is given by $\overline{\nu_i} = \overline{\nu} = 0$ and corresponds to the IF-plane in Fig. 2.

The Diophantine solution of equation (15) is given by,

$$\begin{bmatrix} i \\ j \\ k \end{bmatrix} = \begin{bmatrix} 149 & 0 & 154 \\ -1533 & -115 & -115 \\ 1533 & 124 & 0 \end{bmatrix} \begin{bmatrix} \overline{\nu_i} \\ \alpha \\ \beta \end{bmatrix} \tag{16}$$

Similarly, all $\overline{\nu}$-plane are parallel. The shortest distance between two consecutive planes is about 0.48. Symmetrical to the central zero ionosphere plane ($\overline{\nu}$=0), they are located at constant distances of the planes having a ionosphere amplification factor of $-\overline{\nu}$ and $\overline{\nu}$, respectively.

3) INTERSECTION OF LANE PLANES AND IONOSPHERE PLANES

We look for the intersection between an arbitrary lane plane given by its lane-number m and an arbitrary ionosphere plane given by its ion-number $\overline{\nu_i}$. By introducing the parameterized form of an ionosphere plane (16) in the m-plane of equation (8), it obtains,

$$2151\alpha + 10491\beta = m - 9149\overline{\nu_i} \tag{17}$$

An explicit solution is obtained by solving the Diophantine equation $717\alpha + 3497\beta = p$,

$$\begin{bmatrix} \alpha \\ \beta \end{bmatrix} = \begin{bmatrix} 1073 & 3497 \\ -220 & -717 \end{bmatrix} \begin{bmatrix} p \\ s \end{bmatrix} \tag{18}$$

By substituting equation (18) into equation (16) one obtains an explicit solution for the combination, which is of the type,

$$\begin{bmatrix} i \\ j \\ k \end{bmatrix} = \begin{bmatrix} 149 & -33880 & -110418 \\ -1533 & -98095 & -319700 \\ 1533 & 133052 & 433628 \end{bmatrix} \begin{bmatrix} \overline{\nu_i} \\ p \\ s \end{bmatrix} = \overrightarrow{x}_s + s\delta\overrightarrow{i} \tag{19}$$

where s is an arbitrary integer.

The i–j–k space is converted into the m–$\overline{\nu_i}$–s spacing. We assume that the observation noise should be lowest to fix the value of s. This can be done by first calculating a real value for s [22].

$$s = round(s_{real}) = round\left(\frac{\delta\overrightarrow{i}^T\overrightarrow{x}_s}{\delta\overrightarrow{i}^T\delta\overrightarrow{i}}\right) \tag{20}$$

When m and $\overline{\nu}$ are given, the combination, which is on the m–$\overline{\nu}$ line and nearest to the origin in the i-j-k space, is unique. Namely, the combination (i, j, k) is unique for a given integer pair of m and $\overline{\nu}$.

B. PROPAGATION OF THE OBSERVATION NOISE

For the purpose of simplicity, the noises on all three frequencies expressed in either meter or cycle are the same. It corresponds to the case where a phase lock loop (PLL) is able to track the carrier-phase with an uncertainty described by a standard deviation of typically 0.1–1% [35]. Assuming statistical independence, the combined noise, ε_{c_L} in L, and ε_{c_Φ} in Φ, are expressing in the equations (21) and (22), where ε_{c_L} and ε_{c_Φ} are the noise variance with respect to meter and cycle on a single carrier observation. μ denotes the noise amplification factor with respect to meter (NAPM), and $\overline{\mu}$ is defined as a noise amplification factor with respect to cycle (NAPC).

$$\varepsilon_{c_L} = \frac{\sqrt{(if_1)^2 + (jf_2)^2 + (kf_3)^2}}{if_1 + jf_2 + kf_3} \varepsilon_{0_L} \tag{21}$$

or

$$\varepsilon_{c\Phi} = \sqrt{i^2 + j^2 + k^2}\varepsilon_{0\Phi} \tag{22}$$

where

$$\mu = \frac{\sqrt{(if_1)^2 + (jf_2)^2 + (kf_3)^2}}{if_1 + jf_2 + kf_3} \tag{23}$$

$$\overline{\mu} = \sqrt{i^2 + j^2 + k^2} \tag{24}$$

We assume that the noises on all three frequencies expressed in cycle are the same to describe the noise level for BDS-3 [36]. According to equations (24), if the observation noise of the combination is especially small, we know that except for the origin, the better integer pairs for us to choose is the one that near the origin as much as possible.

C. OPTIMALITY PRINCIPLES CONSIDERING IFB

If the IFB is deemed to be a time dependent quantity, its time-variant characteristic is mainly related to the satellite clock bias. Hence, the IFB can be treated as the time-varying satellite inter-frequency clock bias (IFCB) and the constant part is the inter-frequency hardware bias (IFHB).

Generally, the hardware bias is considered constant, although the DCB has variation feature in the long term [37]. Considering all these aspects, the 1-year IFHB series is modeled with a l-order polynomial function.

$$IFHB^s = \sum_{n=0}^{l} \left(d_n t^n\right) \tag{25}$$

where d_n is the coefficient of the n-order term.

The IFCB can be illustrated by a combined linear and fourth-order harmonic function [38].

$$IFCB^s(t) = d + et + \sum_{i=1}^{4} \lambda_i \sin\left(\frac{2\pi}{T_i}t + \theta_i\right) \tag{26}$$

where d is a constant, e is the coefficient of linear term, i is the order of the harmonics, Ti is the period, θ_i is initial carrier-phase offset, and λ_i is the amplitude. It is important to determine the periods of all orders for describing the IFCB with a high-order harmonics-based composite function.

A harmonic analysis using a fast Fourier transformation (FFT) based on the single-day IFCBs of PRN01 and PRN25 showed that the IFCB varies with apparent periods of 12 h, 6 h, and 8 h [39].

Usually IFB is estimated as a constant IFCB in daily PPP solution [28], [40]. It leads that estimated IFB has a residual error. The combination need consider the influence of the residual error. The combination IFB_c is shown as follow.

$$IFB_c = \frac{kf_3}{if_1 + jf_2 + kf_3} IFB \tag{27}$$

$$w = \frac{kf_3}{if_1 + jf_2 + kf_3} \tag{28}$$

$$\overline{w} = \frac{kf_3}{f_1} = 0.8052k \tag{29}$$

where w is the IFB amplification factor with respect to meter (IFBAFM), $\overline{w}$ is the IFB amplification factor with respect to cycle (IFBAFC).

The absolute value of coefficient of the third observation k is proportional to IFB [28]. To reducing indirect impact on PPP performance during time dependent variables' amplification, the absolute value of coefficient of the third observation k needs to be small.

IV. SEARCHING METHOD FOR OPTIMAL COMBINATIONS

A. BASIC SEARCHING CONSTRAINTS

To fix the ambiguity accurately, optimal combination is a low observation noise, a weak ionosphere, a low frequency, and a low IFB. But these properties can not be implemented at the same time. We only limit the bound of capabilities to find a feasible set. The constraints for optimal combinations can be illustrated as follows.

1) COEFFICIENTS CONSTRAINT

As already pointed out in equation (24), the further the coefficients i, j, and k are from the origin, the higher the noise amplification factor. The limiting coefficients i, j, and k can roughly limit the observation noise.

$$\begin{cases} bound_{i,down} < i < bound_{i,up} \\ bound_{j,down} < j < bound_{j,up} \\ bound_{k,down} < k < bound_{k,up} \end{cases} \tag{30}$$

2) LANE-NUMBER CONSTRAINT

Lane-number m determines the combining frequency as known in equation (6). A low frequency can obtain a long wavelength. In the case of constant noise, long wavelength is easier to fix the ambiguity. Lane-number m is limited as follow.

$$bound_{m,down} < m < bound_{m,up} \tag{31}$$

3) IONOSPHERE CONSTRAINT

Ionosphere delay is also an important factor for ambiguity-fixing as well as observation noise. Ionosphere amplification factor directly reflects the value of the combining ionosphere delay and is limited by the below equation.

$$bound_{\overline{v},down} < \overline{v} < bound_{\overline{v},up} \tag{32}$$

4) NOISE CONSTRAINT

Limiting noise amplification factor is the most direct way to limit observation noise. But the bounds of noise amplification factor are not easy to be determined. Because noise amplification factor is far less than constraint parameters in equations (30)–(32). A small change in the boundary may eliminate some feasible solutions. The noise constraint is usually used for accurate search and posterior search.

5) IFB CONSTRAINT

Limiting IFB amplification factor is the most direct way to limit IFB, similar to noise. But IFB amplification factor

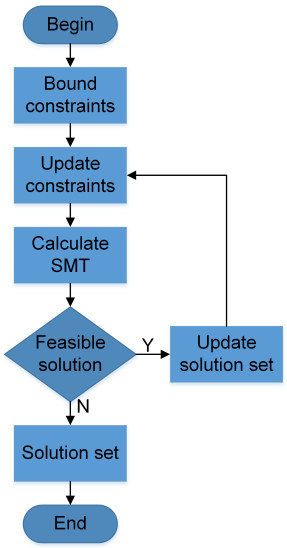

FIGURE 3. SMT-based searching algorithm.

can not be limited with a constant threshold. The threshold is related to Lane-number m. So we use IFB amplification factor for accurate search and posterior search after the rough solution set is found out by a searching algorithm.

B. SMT-BASED SEARCHING ALGORITHM

According to the above constraints, TSA obtains the feasible set by searching the whole range of coefficients i, j, and k. It leads that the processing time is too long. But TSA is well for weak constraint, where there is no limit for the ionosphere amplification factor, the lane-number m and the sum of coefficients. Because many coefficients i, j, and k in the whole range may be feasible solutions. The optimal algorithm is not as well as TSA. The number of feasible solutions is small for strong coefficients, where there are limits for the ionosphere amplification factor, the lane-number m and the sum of coefficients. Algorithm optimization can take an advantage of fast processing.

SMT checks the satisfiability of logic formulas in first-order formulation with regard to linear integer arithmetic (LA (Z)) or bit-vectors (BV) [41], [42]. The coefficients i, j, and k searching problem is easily expressed in terms of constraint-satisfaction in linear arithmetic and are thus suitable application domains for SMT solvers yices. If one exists for the given searching problem, the SMT algorithms will retrieve a feasible solution which is an ''arbitrary'' one of multiple valid solutions. Each of these valid solutions might have a different impact with regard to observation noise. However, SMT can only fast capture a feasible solution and can not obtain all feasible solutions.

To obtain all feasible solutions by using SMT, the iteration is necessary. The SMT-based searching algorithm (SMTSA) adds a constraint in each iteration to solve the problem about retrieving the whole feasible solutions as shown in Fig. 3. After bound constraints are configured, SMT solver searches for the first feasible solution with bound constraints. If the solution exists, the solution set is updated. Meanwhile, the new solution does not belong to the solution set is regarded as a new constraint. As the constraints are updated, SMT solver searches for another feasible solution with updated constraints. The iteration continues until there is no new feasible solution. At this time, all feasible solutions are searched out and stored in the solution set.

TABLE 1. The combinations with the ionosphere-free (The searching ranges of i, j, and k are from -500 to 500).

Index	i	j	k	m	λ (m)	$\overline{\mu}$
1	-77	-345	434	2283	0.01284	559.741012
2	-77	-230	310	132	0.22201	393.610213
3	0	-115	124	2151	0.01362	169.118302
4	77	-460	434	12774	0.00229	637.091045
5	77	-345	310	10623	0.00276	470.163801
6	77	-230	186	8472	0.00346	305.655034
7	77	-115	62	6321	0.00464	151.650915
8	77	0	-62	4170	0.00703	98.858485
9	77	115	-186	2019	0.01451	231.840462
10	154	-345	248	14793	0.00198	451.934730
11	154	-115	0	10491	0.00279	192.200416
12	154	115	-248	6189	0.00474	313.759462
13	154	345	-496	1887	0.01553	623.503809
14	231	-460	310	21114	0.00139	600.883516
15	231	-230	62	16812	0.00174	331.820735
16	231	-115	-62	14661	0.00200	265.386511
17	231	115	-310	10359	0.00283	403.343526
18	231	230	-434	8208	0.00357	542.786330
19	308	-345	124	23133	0.00127	478.816249
20	308	-115	-124	18831	0.00156	351.375867
21	308	115	-372	14529	0.00202	496.460472
22	385	-460	186	29454	0.00099	628.029458
23	385	-345	62	27303	0.00107	520.666880
24	385	-230	-62	25152	0.00117	452.735022
25	385	-115	-186	23001	0.00127	442.770821
26	385	115	-434	18699	0.00157	591.443996
27	462	-115	-248	27171	0.00108	536.817474
28	462	115	-496	22869	0.00128	687.520909

C. IONOSPHERE-FREE COMBINATIONS IN THE PPP-AR

In the TCAR method, especially in the second step which is the wide-lane AR, the wide-lane ambiguity fixed success rate is higher than 98% in DD application [14]. But it is difficult to converge for PPP, because it is not possible to eliminate its error characteristics which is complex and difficult, and non-integer characteristic of its ambiguities.

To allow rapid-to-instantaneous ambiguity resolution in PPP, the required accuracy of the ionoshperic corrections must be better than a few centimeters [34]. So we had better use the constraints which are the ionosphere-free near the origin in the ambiguity resolution as shown in Table 1, where all feasible solutions F are linearly independent. Namely, for $(i_1, j_1, k_1), (i_2, j_2, k_2) \in F$, it has

$$i_1 j_2 \neq i_2 j_1 || j_1 k_2 \neq j_2 k_1 || k_1 i_2 \neq k_2 i_1 \tag{33}$$

But the realistic situation is that the absolute value of the combining integers satisfied these constraints are all numerically large quantities. That is to say, the large absolute values will make high combination noise, so as to increase the

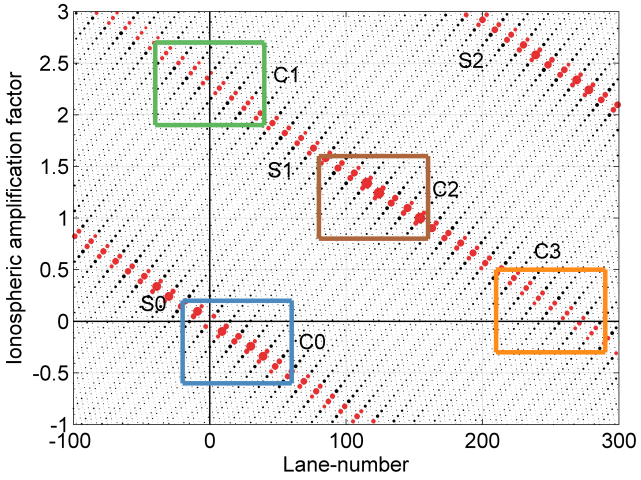

FIGURE 4. Integer linear combinations in the plane defined by m and $\overline{\nu}$. (Combinations with $\overline{w} < 5$ are red, others are black.)

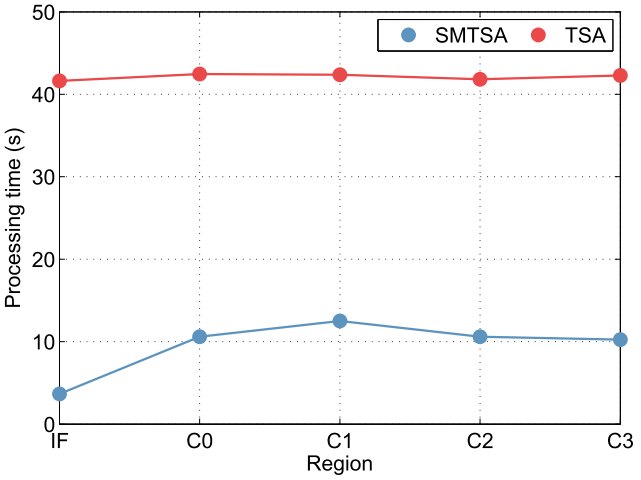

FIGURE 5. Processing time for SMTSA and TSA in case of strong constraints.

convergence time of PPP. Hence, we had better compromise and consider the case of the weak ionosphere constraint.

Nonetheless, the simple weak ionospheric carrier-phase combination constraint like in DD is not satisfy the PPP-AR. But using the pseudorange to counteract the weak ionosphere error caused by carrier-phase integer combination is a possible and feasible way in PPP [33].

V. COMBINATORIAL OPTIMIZATION EXPERIMENT

A. THE FEASIBLE REGION FOR COMBINATIONS

As mentioned in the previous section, we can make some compromises to use the individual or combining pseudorange observations in the carrier-phase combinations to achieve the ionosphere-free purpose and effectiveness. The noise of a pseudorange observation is too large to have a large combining coefficient in pseudorange observation, so ionosphere in carrier-phase combinations should be small. In other words, the next-best way for PPP AR would be to choose the most interesting combination integers with the characteristics of a weak ionosphere, a long wavelength, a low noise, and a low IFB.

To roughly obtain a low observation noise, we constrain the range for i, j, and k to ± 500. In addition, the range of the ionosphere amplification factor $\overline{\nu}$ is [-1, 3], the range of the lane-number m is [-100, 300]. The resulting combinations in the m–$\overline{\nu}$ plane are shown in Fig. 4, where the point varies in inverse proportion to the noise amplification factor $\overline{\mu}$. The low noise axes S0 (i + j + k =0), S1 (i + j + k = 1), and S2 (i + j + k = 2) are visible.

There are three combinations chosen for TCAR or CIR, the three combinations must be independent. It is equivalent that the determinant of the 3×3 combination matrix Z is ± 1 as well as one of dual-frequency combination examined by Teunissen [43]. Teunissen explained that a square matrix containing only integer entries has an integer inverse only if its determinant is ± 1.

TABLE 2. Processing capability for TSA and SMTSA.

Subset	solution number	TSA (s)	SMTSA (s)
IF	28	41.622	3.650
C0	88	42.448	10.655
C1	88	42.370	12.496
C2	89	41.824	10.592
C3	87	42.276	10.234

In triple-frequency ambiguity resolution, the ambiguities of the original observations can only be recovered if all three ambiguities of three independent linear combinations are resolved. Although many combinations in the S0 group have good characteristics, only two independent combinations can be chosen from the i+j+k=0 plane. The third combination belongs to i+j+k =1 plane [22]. The three combinations are from S0 and S1.

B. AVAILABILITY VERIFICATION FOR SMTSA

The feasible solutions in the four colored rectangles correspond to regions of interest are respectively calculated by SMTSA and TSA to analyze the performance of the two algorithms in the case of strong constraints, where the amplitude of the ionosphere amplification factor and the lane-number m are respectively 0.8 and 80 so that the number of feasible solutions is less than 100. The processing time is shown in Fig. 5, where IF is all feasible ionosphere-free combinations with the range for i, j, and k to ± 500. C0 is the subset of S0 in the blue region, C1-C3 are subsets of S1 in the green, brown, and orange regions, respectively. The results shows that SMTSA has faster processing time than TSA in the all cases of strong constraints.

The processing time for TSA and SMTSA is shown in Table 2, where the processing time for SMTSA is related to the number of feasible solutions. The results show that maximum processing time for each solution is 0.142s. According to rough calculation, SMTSA has a faster processing time

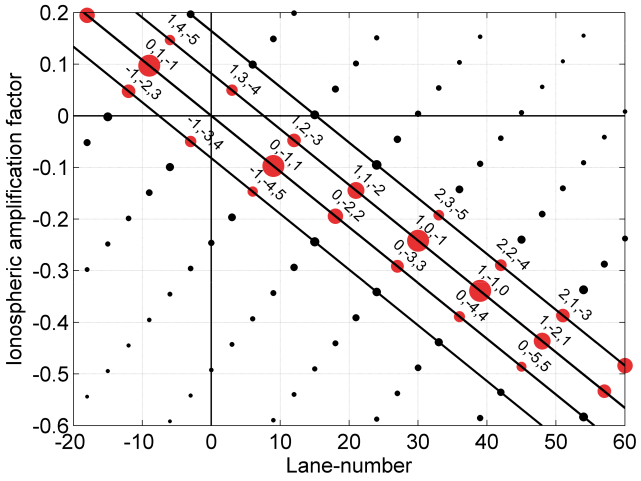

FIGURE 6. The combinations near the origin of the m–$\overline{\nu}$ plane in the S0 group. (Combinations with $w < 5$ are red, others are black.)

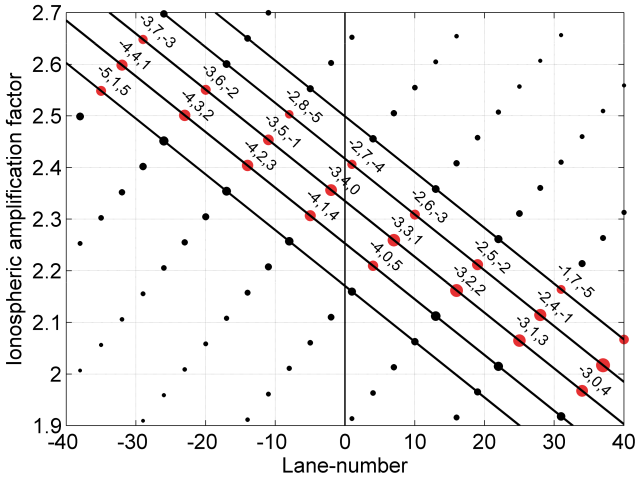

FIGURE 7. The combinations crossing the line m=0 in C1. (Combinations with $w < 5$ are red, others are black.)

TABLE 3. The combinations with an ionosphere-free, a long wavelength and a low noise characteristics in the S0 group.

Index	i	j	k	m	λ (m)	$\overline{\mu}$	$\overline{\nu}$
1	-1	-4	5	6	4.884	6.481	-0.147
2	0	-1	1	9	3.256	1.414	-0.097
3	1	3	-4	3	9.768	5.099	0.050
4	1	2	-3	12	2.442	3.742	-0.048
5	1	1	-2	21	1.395	2.449	-0.145
6	1	0	-1	30	0.977	1.414	-0.242
7	1	-1	0	39	0.751	1.414	-0.339
8	1	-2	1	48	0.611	2.449	-0.436
9	2	5	-7	15	1.954	8.832	0.002
10	2	3	-5	33	0.888	6.164	-0.192
11	2	2	-4	42	0.698	4.899	-0.289
12	2	1	-3	51	0.575	3.742	-0.387
13	3	10	-13	0	Inf	16.673	0.246

than TSA, if the number of feasible solutions is less than 297. It is far larger than the number of feasible solutions in case of strong constraints. SMTSA can search optimal combinations in case of strong constraints rapidly and effectively.

C. THE EXTRA-WIDE-LANE AND WIDE-LANE COMBINATIONS

The blue region C0 is magnified and illustrated in Fig. 6. It is near the origin of the m–$\overline{\nu}$ plane, and crosses the line $\overline{\nu} = 0$ and the line m=0 at the same time. C0 is the wide-lane region characterized by a low ionosphere amplification factor, a long wavelength and a low noise. Table 3 summarizes these combinations and their relevant parameters. When we search the region C0, $k = -i - j$, the range of i, j can limited in $i \in [-31, 31]$ and $j \in [-62, 62]$, the proof can be seen in the appendix.

For extra-wide-lane combinations, long wavelength combinations are (-1, -4, 5), (0, 1, -1), and (1, 3, -4). But combination (-1, -4, 5) has large observation noise. Meanwhile, combination (1, 3, -4) has a larger coefficient k than combination (0, 1, -1). So the combination (0, 1, -1) is the optimal extra-wide-lane combination. The combination (1, 3, -4) can be used as an alternative.

There are four combinations (combinations 4–7 in Table 3) for wide-lane combination, where combination (1, 2, -3) has a very small ionosphere amplification factor, and combination (1, -1, 0) does not have IFB and is usually used in GPS. Although the combination (1, 3, -4) is an alternative extra-wide-lane combination, it can be regarded as a wide-lane combination.

D. THE NARROW-LANE COMBINATION

Considering a low ionosphere amplification factor, a long wavelength, a low observation noise, and a low IFB amplification factor, the three special regions are chosen to select feasible narrow-lane combinations.

1) THE REGION CROSSING THE LANE-NUMBER AXIS

When the requirement of long wavelength is considered, the green region C1 is magnified and shown in Fig. 7, which is across the line m=0. In this region, the range of $\overline{\nu}$ is about 1.9–2.7, and the range of the wavelengths is about 0.7–29.3 m.

Table 4 lists these combinations and the relevant parameters. The result shows that both combinations $(-2, 8, -5)$ and $(-2, 6, -3)$ have long wavelengths. But their noises are so large that they are unsuitable as narrow-lane combination. The combinations $(-2, 7, -4)$ and $(-3, 4, 0)$ have long wavelengths and low noises. Considering the IFB, the combination $(-3, 4, 0)$ is the optimal narrow-lane combination in C1.

2) THE REGION NEAR THE ORIGIN

The brown region C2 is near the origin of the m–$\overline{\nu}$ plane in the S1 group, and the region has a long distance from the line $\overline{\nu} = 0$ and the line m=0 at the same time. This region is magnified and presented in Fig. 8. In this region, the range of $\overline{\nu}$ is about 0.8–1.6, and the range of the wavelengths is

TABLE 4. Optimal combinations near the line m=0 in C1.

Index	i	j	k	m	λ (m)	$\overline{\mu}$	$\overline{\nu}$
1	-2	8	-5	-8	-3.663	9.644	2.503
2	-2	7	-4	1	29.305	8.307	2.406
3	-2	6	-3	10	2.931	7.000	2.309
4	-3	4	0	-2	-14.653	5.000	2.357
5	-3	3	1	7	4.186	4.359	2.259
6	-4	1	4	-5	-5.861	5.745	2.307
7	-4	0	5	4	7.326	6.403	2.210

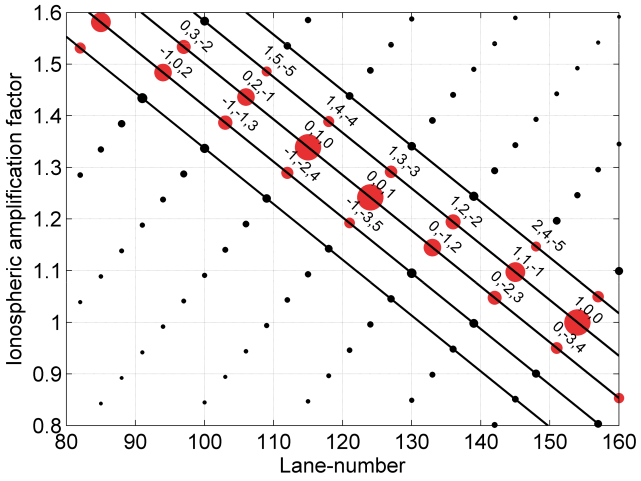

FIGURE 8. The combinations near the origin of the m–$\overline{\nu}$ plane in C2. (Combinations with $w < 5$ are red, others are black.)

TABLE 5. The combinations near the origin in C2.

Index	i	j	k	m	λ (m)	$\overline{\mu}$	$\overline{\nu}$
1	-1	1	1	85	0.345	1.732	1.581
2	-1	0	2	94	0.312	2.236	1.484
3	0	2	-1	106	0.276	2.236	1.436
4	0	1	0	115	0.255	1.000	1.339
5	0	0	1	124	0.236	1.000	1.242
6	0	-1	2	133	0.220	2.236	1.145
7	1	1	-1	145	0.202	1.732	1.097
8	1	0	0	154	0.190	1.000	1.000
9	1	-1	1	163	0.180	1.732	0.903

about 18–37 cm. Both ionosphere amplification factor and lane-number are close to those of the original observations.

The three original observations (1, 0, 0), (0, 1, 0), and (0, 0, 1) have the lowest noise as shown in Table 5. The other combinations in this region have similar $\overline{\nu}$ and m values, but they have more noise. So the only interesting combinations are the original observations.

3) THE REGION CROSSING THE IONOSPHERE–FREE AXIS

When a small ionosphere amplification factor is kept, we should search in the orange region C3 crossing the line $\overline{\nu} = 0$ as shown in Fig. 9. In this region, the range of $\overline{\nu}$ is about -0.3–0.5, and the range of the wavelengths is about 10–14 cm.

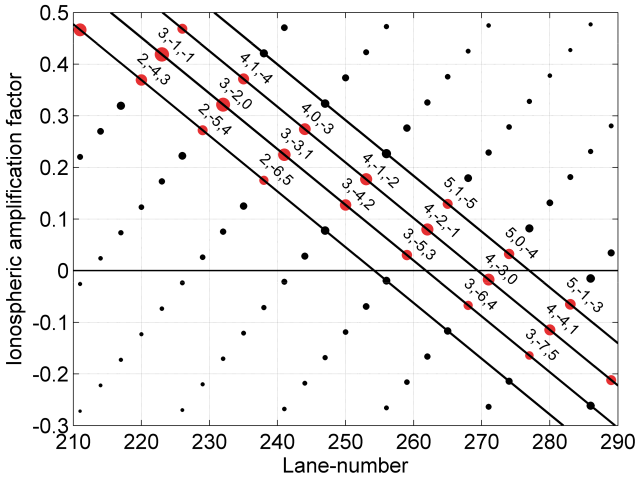

FIGURE 9. The combinations crossing the line $\overline{\nu = 0}$ in C3. (Combinations with $\overline{w} < 5$ are red, others are black.)

TABLE 6. Optimal combinations near the line $\overline{\nu = 0}$ in C3.

Index	i	j	k	m	λ (m)	$\overline{\mu}$	$\overline{\nu}$
1	2	-6	5	238	0.123	8.062	0.175
2	3	-4	2	250	0.117	5.385	0.127
3	3	-5	3	259	0.113	6.557	0.030
4	3	-6	4	268	0.109	7.810	-0.067
5	3	-7	5	277	0.106	9.110	-0.164
6	4	-1	-2	253	0.116	4.583	0.177
7	4	-2	-1	262	0.112	4.583	0.080
8	4	-3	0	271	0.108	5.000	-0.017
9	4	-4	1	280	0.105	5.745	-0.115

TABLE 7. Feasible narrow-lane combinations in the S1 group.

Index	i	j	k	m	λ (m)	$\overline{\mu}$	$\overline{\nu}$
1	-2	7	-4	1	29.305	8.307	2.406
2	-3	4	0	-2	-14.653	5.000	2.357
3	0	1	0	115	0.255	1.000	1.339
4	0	0	1	124	0.236	1.000	1.242
5	1	0	0	154	0.190	1.000	1.000
6	3	-4	2	250	0.117	5.385	0.127
7	4	-1	-2	253	0.116	4.583	0.177
8	4	-2	-1	262	0.112	4.583	0.080
9	4	-3	0	271	0.108	5.000	-0.017
10	4	-4	1	280	0.105	5.745	-0.115

Table 6 lists these combinations and the relevant parameters. The useful combinations (3, -4, 2), (4, -1, -2), (4, -2, -1), (4, -3, 0), and (4, -4, 1) have small $\overline{\nu}$ values and low noises.

4) FEASIBLE NARROW-LANE COMBINATIONS

All feasible narrow-lane combinations are shown in Table 7. The results show that the combination (-2, 7, -4) has the largest IFB amplification factor $\overline{w}$, but its wavelength is so long that the influence of $\overline{w}$ can be ignored. Considering combinations (-2, 7, -4) and (-3, 4, 0) have large ionosphere amplification factor, they can be only used as narrow-lane combinations. Furthermore, considering IFB amplification factor $\overline{w}$, combinations (-3, 4, 0), (0, 1, 0), (1, 0, 0)

and (4, -3, 0) are better than others. Considering a weak ionosphere, a long wavelength, a low noise, and a low IFB, combinations (0, 1, 0), (-2, 7, -4) and (-3, 4, 0) are optimal narrow-lane combinations. The others are second-choice in Table 7.

VI. CONCLUSION

The carrier-phase integer combination is critical prerequisite for TCAR and CIR to fix ambiguity. Considering IFB in triple-frequency observations, we presented some optimal carrier-phase integer combinations for BDS-3.

Integer ambiguities can be characterized by four parameters: the lane-number m, the ionosphere amplification factor $\overline{\nu}$, the noise amplification factor $\overline{\mu}$, and the IFB amplification factor $\overline{w}$. We presented the mathematical model of the parameters. To simplify searching carrier-phase integer combination, we proved that i–j–k plane can be converted to m–$\overline{\nu}$ plane under the assumption of a low noise in BDS-3.

And then all searching constraints are analyzed. Meanwhile, the IFB constraint was added to select optimized carrier-phase integer combinations. Thereafter, the SMT-based searching algorithm was proposed to decrease the processing time of searching task. Moreover, we analyzed the carrier-phase integer combinations with ionosphere-free, and they have high noise and narrow-lane. The IF constraint is not suitable for PPP-AR.

Finally, combinatorial optimization experiments were realized to find optimized carrier-phase integer combinations according to the above theory and method.

APPENDIX

For the extra-wide-lane and wide-lane combinations, it has

$$0 < if_1 + jf_2 + kf_3 < f_2 \tag{34}$$

The coefficient k can be determined by i and j, then the bounds of the coefficient k are shown as follow.

$$\frac{-if_1 - jf_2}{f_3} < k < \frac{(1-j)f_2 - if_1}{f_3} \tag{35}$$

From the above equation, the absolute value of the difference between the maximum and the minimum of the coefficient k is 0.927. In other words, the integer-value of k is between its maximum and minimum real-value.

We assume that k is the one that round up to an integer of $k_{\min}$, it obtains the following formula [44].

$$0 < 30i + 115j + 124\left\lceil -\frac{15i}{62} - \frac{115j}{124}\right\rceil < f_2 \tag{36}$$

The coefficients i and j have an obvious periodicity (62 and 124), respectively. Namely, $i \in [-31, 31]$, $j \in [-62, 62]$.

ACKNOWLEDGMENT

The authors wish to acknowledge the efforts of all entities contributing to MGEX. All products used in this work are openly available in ftp://igs.ign.fr/. The colleagues who provided insight and stimulating discussions that greatly assisted in the preparation of this paper. The authors gratefully acknowledge the anonymous reviewers for carefully reading the paper and providing constructive comments.

REFERENCES

[1] J. F. Zumberge, M. B. Heflin, D. C. Jefferson, M. M. Watkins, and F. H. Webb, "Precise point positioning for the efficient and robust analysis of GPS data from large networks," *J. Geophys. Res.*, vol. 102, no. B3, pp. 5005–5017, 1997, doi: 10.1029/96JB03860.

[2] J. Kouba and P. Héroux, "Precise point positioning using IGS orbit and clock products," *GPS Solutions*, vol. 5, no. 2, pp. 12–28, 2001, doi: 10.1007/PL00012883.

[3] S. Bisnath and Y. Gao, "Current state of precise point positioning and future prospects and limitations," in *Proc. Observing Our Changing Earth, Int. Assoc. Geodesy Symposia*. Berlin, Germany: Springer-Verlag, 2009, pp. 615–623, doi: 10.1007/978-3-540-85426-5_71.

[4] M. Ge, G. Gendt, M. Rothacher, C. Shi, and J. Liu, "Resolution of GPS carrier-phase ambiguities in precise point positioning (PPP) with daily observations," *J. Geodesy*, vol. 82, no. 7, pp. 389–399, 2008, doi: 10.1007/s00190-007-0187-4.

[5] P. Collins, F. Lahaye, P. Héroux, and S. Bisnath, "Precise point positioning with ambiguity resolution using the decoupled clock model," in *Proc. 21st Int. Tech. Meeting Satell. Division Inst. Navigat.*, Savannah, Georgia, 2008, pp. 1315–1322.

[6] D. Laurichesse, F. Mercier, J.-P. Berthias, P. Broca, and L. Cerri, "Integer ambiguity resolution on undifferenced GPS phase measurements and its application to PPP and satellite precise orbit determination," *Navigation*, vol. 56, no. 2, pp. 135–149, 2009.

[7] P. Teunissen, "The least-squares ambiguity decorrelation adjustment: A method for fast GPS integer ambiguity estimation," *J. Geodesy*, vol. 70, nos. 1–2, pp. 65–82, 1995, doi: 10.1007/bf00863419.

[8] G. Blewitt, "Carrier phase ambiguity resolution for the global positioning system applied to geodetic baselines up to 2000 km," *J. Geophys. Res., Solid Earth*, vol. 94, no. B8, pp. 10187–10203, 1989, doi: 10.1029/jb094ib08p10187.

[9] P. Teunissen, P. Joosten, and C. Tiberius, "A comparison of TCAR, CIR and LAMBDA GNSS ambiguity resolution," in *Proc. 15th Int. Tech. Meeting Satell. Division Inst. Navigat.* Portland, OR, USA: ION, 2002, pp. 2799–2808.

[10] P. J. G. Teunissen, "An optimality property of the integer least-squares estimator," *J. Geodesy*, vol. 73, no. 11, pp. 587–593, 1999, doi: 10.1007/s001900050269.

[11] B. Forssell, M. Martín-Neira, and R. Harris, "Carrier phase ambiguity resolution in GNSS-2," in *Proc. ION GPS*, vol. 10, 1997, pp. 1727–1736.

[12] J. Jung, P. Enge, and B. Pervan, "Optimization of cascade integer resolution with three civil GPS frequencies," in *Proc. 13th Int. Tech. Meeting Satell. Division Inst. Navigat.*, Salt Lake City, UT, USA, 2000, pp. 2191–2200.

[13] S. Verhagen, "Analysis of integer ambiguity resolution algorithms," *Eur. J. Navigat.*, vol. 2, no. 4, pp. 38–50, 2004.

[14] P. J. Teunissen, "Gnss ambiguity bootstrapping: Theory and application," in *Proc. Int. Symp. Kinematic Syst. Geodesy, Geomatics Navigat.*, Banff, Canada, 2001, pp. 246–254.

[15] P. Teunissen and D. Odijk, "Rank-defect integer estimation and phase-only modernized GPS ambiguity resolution," *J. Geodesy*, vol. 76, nos. 9–10, pp. 523–535, 2003, doi: 10.1007/s00190-002-0285-2.

[16] S. Han and C. Rizos, "The impact of two additional civilian GPS frequencies on ambiguity resolution strategies," in *Proc. 55th Nat. Meeting US Inst. Navigat., Navigational Technol. 21st Century*, Cambridge, MA, USA, 1999, pp. 28–30.

[17] T. Richert and N. El-Sheimy, "Optimal linear combinations of triple frequency carrier phase data from future global navigation satellite systems," *GPS Solutions*, vol. 11, pp. 11–19, Jan. 2007, doi: 10.1007/s10291-006-0024-x.

[18] Y. Feng, "GNSS three carrier ambiguity resolution using ionosphere-reduced virtual signals," *J. Geodesy*, vol. 82, no. 12, pp. 847–862, 2008, doi: 10.1007/s00190-008-0209-x.

[19] S. Gu, Y. Lou, C. Shi, and J. Liu, "Beidou phase bias estimation and its application in precise point positioning with triple-frequency observable," *J. Geodesy*, vol. 89, no. 10, pp. 979–992, 2015, doi: 10.1007/s00190-015-0827-z.

[20] P. Li, X. Zhang, M. Ge, and H. Schuh, "Three-frequency BDS precise point positioning ambiguity resolution based on raw observables," *J. Geodesy*, vol. 92, no. 12, pp. 1357–1369, 2018, doi: 10.1007/s00190-018-1125-3.

[21] C. Deng, W. Tang, J. Cui, M. Shen, Z. Li, Z. Xuan, and Y. Zhang, "Triple-frequency code-phase combination determination: A comparison with the hatch-melbourne-wübbena combination using BDS signals," *Remote Sens.*, vol. 10, no. 2, p. 353, 2018, doi: 10.3390/rs10020353.

[22] M. Cocard, S. Bourgon, O. Kamali, and P. Collins, "A systematic investigation of optimal carrier-phase combinations for modernized triple-frequency GPS," *J. Geodesy*, vol. 82, no. 9, pp. 555–564, 2008, doi: 10.1007/s00190-007-0201-x.

[23] X. Zhang and X. He, "BDS triple-frequency carrier-phase linear combination models and their characteristics," *Sci. China Earth Sci.*, vol. 58, no. 6, pp. 896–905, 2015, doi: 10.1007/s11430-014-5027-9.

[24] J. Li, Y. Yang, H. He, and H. Guo, "An analytical study on the carrier-phase linear combinations for triple-frequency GNSS," *J. Geodesy*, vol. 91, pp. 151–166, Feb. 2017, doi: 10.1007/s00190-016-0945-2.

[25] X. Zhang and X. Li, "Instantaneous re-initialization in real-time kinematic PPP with cycle slip fixing," *GPS Solutions*, vol. 16, no. 3, pp. 315–327, 2012, doi: 10.1007/s10291-011-0233-9.

[26] J. Geng, X. Meng, A. H. Dodson, M. Ge, and F. N. Teferle, "Rapid re-convergences to ambiguity-fixed solutions in precise point positioning," *J. Geodesy*, vol. 84, no. 12, pp. 705–714, 2010, doi: 10.1007/s00190-010-0404-4.

[27] P. Collins and S. Bisnath, "Issues in ambiguity resolution for precise point positioning," in *Proc. 24th Int. Tech. Meeting Satell. Division Inst. Navigat.*, Portland, OR, USA, 2011, p. 679.

[28] P. Liu, H. Qin, and L. Cong, "The unified form of code biases and positioning performance analysis in global positioning system (GPS)/BeiDou navigation satellite system (BDS) precise point positioning using real triple-frequency data," *Sensors*, vol. 19, no. 11, p. 2469, 2019, doi: 10.3390/s19112469.

[29] F. Guo, X. Zhang, J. Wang, and X. Ren, "Modeling and assessment of triple-frequency BDS precise point positioning," *J. Geodesy*, vol. 90, no. 11, pp. 1223–1235, 2016, doi: 10.1007/s00190-016-0920-y.

[30] H. Li, B. Li, G. Xiao, J. Wang, and T. Xu, "Improved method for estimating the inter-frequency satellite clock bias of triple-frequency GPS," *GPS Solutions*, vol. 20, no. 4, pp. 751–760, 2016, doi: 10.1007/s10291-015-0486-9.

[31] S. Ye, L. Zhao, J. Song, D. Chen, and W. Jiang, "Analysis of estimated satellite clock biases and their effects on precise point positioning," *GPS Solutions*, vol. 22, no. 1, p. 16, 2018, doi: 10.1007/s10291-017-0680-z.

[32] Y. Feng and C. Rizos, "Three carrier approaches for future global, regional and local GNSS positioning services: Concepts and performance perspectives," in *Proc. 18th Int. Tech. Meeting Satell. Division Inst. Navigat.*, vol. 16. Long Beach, CA, USA: Citeseer, 2005, pp. 2277–2278.

[33] J. Geng and Y. Bock, "Triple-frequency GPS precise point positioning with rapid ambiguity resolution," *J. Geodesy*, vol. 87, no. 5, pp. 449–460, 2013, doi: 10.1007/s00190-013-0619-2.

[34] S. Choy, S. Bisnath, and C. Rizos, "Uncovering common misconceptions in GNSS precise point positioning and its future prospect," *GPS Solutions*, vol. 21, no. 1, pp. 13–22, 2017, doi: 10.1007/s10291-016-0545-x.

[35] M. S. Braasch and A. J. van Dierendonck, "GPS receiver architectures and measurements," *Proc. IEEE*, vol. 87, no. 1, pp. 48–64, Jan. 1999, doi: 10.1109/5.736341.

[36] W. Tang, C. Deng, C. Shi, and J. Liu, "Triple-frequency carrier ambiguity resolution for Beidou navigation satellite system," *GPS Solutions*, vol. 18, no. 3, pp. 335–344, 2014, doi: 10.1007/s10291-013-0333-9.

[37] Y. Gao, F. Lahaye, P. Heroux, X. Liao, N. Beck, and M. Olynik, "Modeling and estimation of c1–p1 bias in GPS receivers," *J. Geodesy*, vol. 74, no. 9, pp. 621–626, 2001, doi: 10.1007/s001900000117.

[38] O. Montenbruck, U. Hugentobler, R. Dach, P. Steigenberger, and A. Hauschild, "Apparent clock variations of the block IIF-1 (SVN62) GPS satellite," *GPS Solutions*, vol. 16, no. 3, pp. 303–313, 2012, doi: 10.1007/s10291-011-0232-x.

[39] H. Li, Y. Chen, B. Wu, X. Hu, F. He, G. Tang, and J. Chen, "Modeling and initial assessment of the inter-frequency clock bias for compass GEO satellites," *Adv. Space Res.*, vol. 51, no. 12, pp. 2277–2284, 2013, doi: 10.1016/j.asr.2013.02.012.

[40] A. El-Mowafy, M. Deo, and C. Rizos, "On biases in precise point positioning with multi-constellation and multi-frequency GNSS data," *Meas. Sci. Technol.*, vol. 27, no. 3, 2016, Art. no. 035102, doi: 10.1088/0957-0233/27/3/035102.

[41] C. Barrett and C. Tinelli, "Satisfiability modulo theories," in *Handbook of Model Checking*. Cham, Switzerland: Springer, 2018, pp. 305–343.

[42] R. Sebastiani, "Lazy satisfiability modulo theories," *J. Satisfiability, Boolean Model. Comput.*, vol. 3, pp. 141–224, 2007.

[43] P. J. G. Teunissen, "The invertible GPS ambiguity transformations," *Manuscripta Geodaetica*, vol. 20, no. 6, pp. 489–497, 1995, doi: 10.1109/36.469496.

[44] Y. Wu, "The theory and application on multi-frequency data processing of GNSS 2," Ph.D. dissertation, School Geodesy Gematics, Wuhan Univ., Wuhan, China, 2005.

HONGLEI QIN received the B.S. degree in computer application from the Changchun Institute of Technology, China, in 1996, the M.S. degree in electrical engineering from the Harbin Institute of Technology, China, and the Ph.D. degree in navigation guided and control from Harbin Engineering University, China, in 2001.

He has published over 125 peer-reviewed articles which are indexed by SCI or EI (citation frequency 671) and three books. He is the Leader of Communication, Navigation and Test Laboratory (CNT Lab), Beihang University. He is the Chairman of the Department of Information and Communications Engineering, School of Electronic Information Engineering, Beihang University. Furthermore, he is the Vice Chairman of the Navigation Branch of the Chinese Institute of Electronics and the Vice Chief of the Beijing Key Laboratory of Microwave and Security Applications. Since January 2018, he has been the Vice Chairman of the National Technical Committee on Measurement and Testing for Satellite Navigation Applications. He is currently a Full Professor with Beihang University, China. Moreover, he has presided more than twenty major projects in total, such as the National Natural Science Foundation of China, the National 863 Program, and BDS Key Project. His researches are focused on automatic test systems, fault diagnosis, and satellite navigation.

PENG LIU was born in Baishan, Jilin, China. She received the M.S. degree in signal and information processing from the College of Communication Engineering, Jilin University, in September 2014.

She is currently pursuing the Ph.D. degree in communication and information system with the School of Electronic Information Engineering, Beihang University, China. Her research interests include GNSS, PPP, and its applications, especially, the observation models and ambiguity resolution algorithm.

JIAQING QU received the Ph.D. degree in communication and information systems from Harbin Engineering University, China, in 2010.

He is currently a Senior Engineer with the Shanghai Radio Equipment Research Institute, China. His research interest concerns satellite navigation receivers.

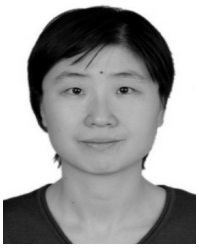

LI CONG received the M.S. degree in control theory and control engineering from Harbin Engineering University, China, in 2004, and the Ph.D. degree in communication and information systems from Beihang University, China, in 2008.

She is currently an Associate Professor with the School of Electronic Information Engineering, Beihang University, China. In this area, she has published over 45 peer-reviewed articles (citation frequency 348) and one book. Her research interests concern satellite navigation, tactical navigation, and integrated navigation.